INTERNATIONAL JOURNAL FOR NUMERICAL METHODS IN FLUIDS
Int. J. Numer. Meth. Fluids 2006; **51**:31–47
Published online 15 November 2005 in Wiley InterScience (www.interscience.wiley.com). DOI: 10.1002/fld.1106

An improved MPS method for numerical simulations of convective heat transfer problems

Shuai Zhang[1,*,†], Koji Morita[2,‡], Kenji Fukuda[2,§] and Noriyuki Shirakawa[3,¶]

[1]*Department of Applied Quantum Physics and Nuclear Engineering, Kyushu University, Fukuoka, Japan*
[2]*Institute of Environmental Systems, Kyushu University, Fukuoka, Japan*
[3]*Nuclear Power Engineering Corporation, Tokyo, Japan*

SUMMARY

An improved moving-particle semi-implicit (MPS) method was developed for numerical simulations of convective heat transfer problems. The MPS method, which is based on particles and their interactions, is a fully Lagrangian particle method for incompressible flows. A new Laplacian model and a new method for treating boundary conditions were proposed to solve numerical difficulties resulting from the original MPS method. Results of several numerical tests show the validity of the improved MPS method with the proposed model and method.

The application of the present MPS method to Rayleigh–Benard convection phenomena demonstrated the effectiveness of the proposed model and method on the numerical simulation of convective heat transfer problems. The dependence of the Nusselt number on the Rayleigh number was in good agreement with an empirical formula. The temperature contour and velocity distribution also agree well with the simulation results obtained with other methods. The roll pattern developed in the horizontal fluid layer as well as the convective heat transfer was successfully simulated with three-dimensional MPS calculations. Copyright © 2005 John Wiley & Sons, Ltd.

KEY WORDS: moving-particle semi-implicit (MPS) method; convective heat transfer; Laplacian model; Rayleigh–Benard convection

1. INTRODUCTION

It is difficult for Eulerian methods to analyse complex geometries and to treat viscous fluid flows without numerical diffusion caused by fluid convection. Lagrangian methods are other

*Correspondence to: Shuai Zhang, Department of Applied Quantum Physics and Nuclear Engineering, Kyushu University, Fukuoka, Japan.
†E-mail: zhang@nucl.kyushu-u.ac.jp
‡E-mail: morita@nucl.kyushu-u.ac.jp
§E-mail: fuku@nucl.kyushu-u.ac.jp
¶E-mail: shirakawa@nupec.or.jp

Contract/grant sponsor: Ministry of Education, Culture, Sports, Science and Technology, Japan

Received 26 April 2005
Revised 16 August 2005
Accepted 23 August 2005

approaches to overcome these problems. A moving-particle semi-implicit (MPS) method [1] is a deterministic Lagrangian method developed for simulating incompressible fluids. In this method, governing equations are discretized based on particle interaction models representing gradient, Laplacian and free surface. Computational grids are unnecessary. Based on the MPS method, a combined grid and particle method, MPS-MAFL [2], which can easily solve flow problems with inlets and outlets, has been formulated. A two-fluid MPS method [3] has been developed extensively for two-phase fluid problems. All these methods have been applied with satisfying results in natural and engineering fields.

However, the original Laplacian model [1] presented in the MPS method would overestimate heat transfer when applied to an energy equation. We also found that it was difficult for the MPS method to obtain numerical stability for natural convection flows with a low Reynolds number or in an enclosure. In addition, the cut-off radius defined in the gradient or the Laplacian models cannot satisfy geometric boundaries because wall boundaries are simulated by one-layer particles with zero velocities. To overcome these problems, in the present paper, we will propose a new Laplacian model for the heat transfer along with a new treatment for thermal and non-slip boundaries.

Rayleigh–Benard convection takes place in a horizontal layer, which is heated from the bottom and cooled from the top. A stable conduction exists for this problem when the temperature difference between the bottom and top boundaries is small enough. When a temperature difference is increased above a certain threshold, the static conduction becomes unstable against any small disturbance, and the system then becomes unstable. Chandrasekhar presented a lucid introduction and thorough coverage of the theory to this phenomenon [4]; and there have been some reviews on experiments and numerical calculations in this particular field [5]. Recently, new technologies have been applied to the study of the role of molecules in macroscopic flow phenomena, for example the molecular dynamics [6], the direct simulation Monte Carlo [7] and the lattice Boltzmann method [8]. Most of these simulations were done in the Euler framework. Smoothed particle applied mechanics, a grid-free Lagrangian method, was used to simulate the Rayleigh–Benard convection to emphasize and discuss the connection between molecular dynamics and continuum mechanics [9]. In this contribution, the MPS method with a new Laplacian model and a new method for treating the boundary conditions will be used to simulate Rayleigh–Benard convection with a range of Rayleigh number.

2. NUMERICAL MODELS AND METHODS FOR MPS

2.1. Governing equations in MPS method

Governing equations for incompressible flows are mass, momentum and energy conservation equations given as follows:

$$\frac{\partial \rho}{\partial t} + \nabla \cdot (\rho \mathbf{u}) = 0 \tag{1}$$

$$\frac{\mathrm{D}\mathbf{u}}{\mathrm{D}t} = -\frac{\nabla p}{\rho} + \upsilon \nabla^2 \mathbf{u} + \mathbf{F} \tag{2}$$

$$\rho c_{\mathrm{p}} \frac{\mathrm{D}T}{\mathrm{D}t} = \lambda \nabla^2 T - q \tag{3}$$

2.1.1. Kernel function. In MPS, the kernel function $w(|\mathbf{r}_j - \mathbf{r}_i|, r_e)$ is chosen as [1]

$$w(|\mathbf{r}_j - \mathbf{r}_i|, r_e) = \begin{cases} \dfrac{r_e}{(|\mathbf{r}_j - \mathbf{r}_i|)} - 1 & (|\mathbf{r}_j - \mathbf{r}_i| < r_e) \\ 0 & (|\mathbf{r}_j - \mathbf{r}_i| \geqslant r_e) \end{cases} \tag{4}$$

$$n^0 = \sum_{j \neq i} w(|\mathbf{r}_j - \mathbf{r}_i|, r_e) \tag{5}$$

where r_e is the cut-off radius. In the present MPS method, it is chosen to be $2.1\Delta l$, where Δl is the initial distance between two particles. With this kernel function, particle clusters can be avoided since the value of kernel function is infinity at $|\mathbf{r}_j - \mathbf{r}_i| = 0$.

2.1.2. Gradient model. Assuming two particles i and j, which possess scalar quantities Φ_i and Φ_j, respectively, the gradient in the MPS method is defined as [1]

$$\langle \nabla \Phi \rangle_i = \frac{d}{n^0} \sum_{j \neq i} \frac{\Phi_j - \Phi_i}{|\mathbf{r}_j - \mathbf{r}_i|^2} (\mathbf{r}_j - \mathbf{r}_i) w(|\mathbf{r}_j - \mathbf{r}_i|, r_e) \tag{6}$$

where d is the number of the space dimension.

Equation (6) can be rearranged as follows:

$$\langle \nabla \Phi \rangle_i = \frac{d}{n^0} \sum_{j \neq i} \frac{\Phi_j - \Phi_i'}{|\mathbf{r}_j - \mathbf{r}_i|^2} (\mathbf{r}_j - \mathbf{r}_i) w(|\mathbf{r}_j - \mathbf{r}_i|, r_e) \tag{7}$$

where $\Phi_i' = \min(\Phi_j)$. Equation (7) is tested to be able to improve numerical stability [1].

2.1.3. Laplacian model. The original Laplacian model in the MPS method is given by Koshizuka and Oka [1]

$$\langle \nabla^2 \Phi \rangle_i = \frac{2d}{n^0 \lambda} \sum_{j \neq i} (\Phi_j - \Phi_i) w(|\mathbf{r}_j - \mathbf{r}_i|, r_e) \tag{8}$$

where

$$\lambda = \frac{\int w(|\mathbf{r}_j - \mathbf{r}_i|, r_e) |\mathbf{r}_j - \mathbf{r}_i|^2 \, \mathrm{d}v}{\int w(|\mathbf{r}_j - \mathbf{r}_i|, r_e) \, \mathrm{d}v} \tag{9}$$

In two dimensions, parameter λ should be

$$\begin{aligned} \lambda &= \frac{2\pi \int_0^\infty w(|\mathbf{r}_j - \mathbf{r}_i|, r_e) |\mathbf{r}_j - \mathbf{r}_i|^3 \, \mathrm{d}|\mathbf{r}_j - \mathbf{r}_i|}{2\pi \int_0^\infty w(|\mathbf{r}_j - \mathbf{r}_i|, r_e) |\mathbf{r}_j - \mathbf{r}_i| \mathrm{d}|\mathbf{r}_j - \mathbf{r}_i|} \\ &\approx \frac{\int_R^{r_e} w(|\mathbf{r}_j - \mathbf{r}_i|, r_e) |\mathbf{r}_j - \mathbf{r}_i|^3 \, \mathrm{d}|\mathbf{r}_j - \mathbf{r}_i|}{\int_R^{r_e} w(|\mathbf{r}_j - \mathbf{r}_i|, r_e) |\mathbf{r}_j - \mathbf{r}_i| \mathrm{d}|\mathbf{r}_j - \mathbf{r}_i|} \end{aligned} \tag{10}$$

where

$$R = \Delta l/\sqrt{\pi} \tag{11}$$

However, it is found that this model would overestimate heat conduction when applied to an energy equation. This will be demonstrated using the numerical test for heat conduction in a homogenous square slab in Section 3.

As we know, the Laplacian model can be derived from the divergence of gradient as

$$\langle \nabla^2 \Phi \rangle_i = \langle \nabla \cdot \nabla(\Phi)_{ij} \rangle_i \tag{12}$$

where the divergence model in the MPS method is

$$\langle \nabla \cdot \boldsymbol{\varphi} \rangle_i = \frac{d}{n^0} \sum_{j \neq i} \frac{(\boldsymbol{\varphi}_j - \boldsymbol{\varphi}_i) \cdot (\mathbf{r}_j - \mathbf{r}_i)}{|\mathbf{r}_j - \mathbf{r}_i|^2} w(|\mathbf{r}_j - \mathbf{r}_i|, r_e) \tag{13}$$

Combining the gradient model and the divergence model, we can obtain the new Laplacian model:

$$\langle \nabla^2 \Phi \rangle_i = \frac{2d}{n^0} \sum_{i \neq j} \frac{\Phi_j - \Phi_i}{|\mathbf{r}_j - \mathbf{r}_i|^2} w(|\mathbf{r}_j - \mathbf{r}_i|, r_e) \tag{14}$$

In the original Laplacian model, it is necessary to use a parameter, λ, which is derived with the central limit theorem. However, mathematical inconsistency in the definition of λ could cause numerical difficulties in calculating the Poisson equation. In contrast, Equation (14) enables us to solve the Poisson equation exactly.

2.1.4. Incompressible model. In the MPS method, each particle possesses the same mass. Therefore, every particle number density n^* should be constant and equal to n^0. Otherwise, we define

$$n^* + n' = n^0 \tag{15}$$

where n' is the correction to the particle number density. The following can be derived:

$$\frac{1}{\Delta t} \frac{n'}{n^0} = -\nabla \cdot \mathbf{u}' \tag{16}$$

$$\mathbf{u}' = -\frac{\Delta t}{\rho} \nabla p^{n+1} \tag{17}$$

where $\mathbf{u}'$ is the velocity correction value and $n+1$ means the next time step number. As a result, we get the following pressure Poisson equation [1]:

$$\langle \nabla^2 p^{n+1} \rangle_i = -\frac{\rho}{\Delta t^2} \frac{\langle n^* \rangle_i - n^0}{n^0} \tag{18}$$

To improve calculation stability, especially for flows in an enclosure, the equation is modified as [10]

$$\langle \nabla^2 p^{n+1} \rangle_i = \alpha_1 \frac{\rho}{\Delta t} \nabla \cdot \langle \mathbf{u}^* \rangle - \alpha_2 \frac{\rho}{\Delta t^2} \frac{\langle n^* \rangle_i - n^0}{n^0} \tag{19}$$

with

$$\alpha_1 + \alpha_2 = 1 \tag{20}$$

where the parameters α_1 and α_2 are chosen as 0.8 and 0.2, respectively, in the present calculations. $\mathbf{u}^*$ is the temporal velocity.

Equation (19) can be solved by the incomplete Cholesky conjugate gradient (ICCG) method, which is robust and fast for calculations with a large number of particles.

2.2. Time integration

The MPS method separates calculations into two stages, explicit and implicit stages, in each time step. In the explicit stage, particles move with the viscosity and external forces that are explicitly calculated by

$$\mathbf{u}_i^* = \mathbf{u}_i^n + \Delta t(\upsilon \nabla^2 \mathbf{u}_i^n + \mathbf{F}_i) \tag{21}$$

$$\mathbf{r}_i^* = \mathbf{r}_i^n + \Delta t \mathbf{u}_i^* \tag{22}$$

In the implicit stage, velocity is corrected with Equation (17) to keep the conservation of the momentum equation. Pressure is obtained with Equation (19) using the ICCG method. Time step is controlled in the computation to satisfy the following Courant condition:

$$\Delta t \leqslant 0.2 \frac{\Delta l}{u_{\max}} \tag{23}$$

where Δl is the initial distance between two particles, and $u_{\max}$ is the maximal velocity among all particles.

2.3. Boundary conditions

The original method of treating boundary conditions in MPS simulates the wall by one-layer of fixed particles with zero velocities. Other two-layer dummy particles are used for calculating the number density of the wall particles to distinguish particles on the free surface from wall particles in pressure Poisson equation. However, since the cut-off radius for both gradient and Laplacian models for the pressure Poisson equation is larger than Δl, the cut-off radius is not in agreement with the geometric boundaries. In the original MPS method, the pressure and velocity of a dummy particle are fixed as zero to solve this problem. Further, the velocities of wall and dummy particles are defined as zero to retain the non-slip boundary condition when calculating the viscosity force. However, zero velocity should be physically kept on the wall. The same difficulty will be encountered in the case of the heat transfer calculations near the wall.

To overcome such difficulties in treating boundary conditions, we define one-layer wall particles and fictitious particles that are reflected from the fluid particles by the wall, as shown in Figure 1. Fluid particles interact with other fluid, wall and fictitious particles in the calculations of viscosity force and heat transfer. The fictitious particles have the same magnitude of velocities as the corresponding fluid particles, but in the opposite direction. The thermal boundary condition can be easily satisfied with this treatment. For the Dirichlet boundary condition, the average temperature of a fluid particle and the corresponding fictitious particle is kept the same as the temperature value on the wall. For the Neumann boundary

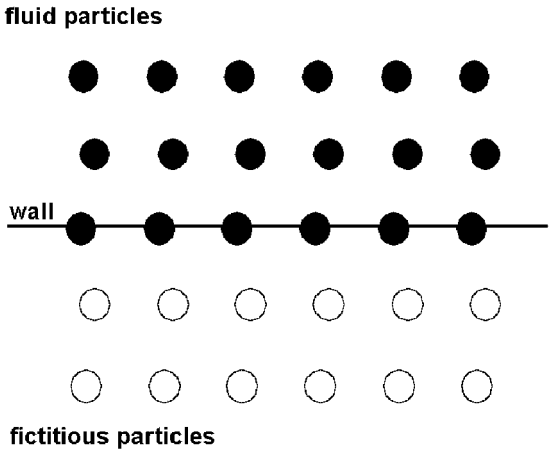

Figure 1. Numerical treatment of thermal and velocity boundary conditions.

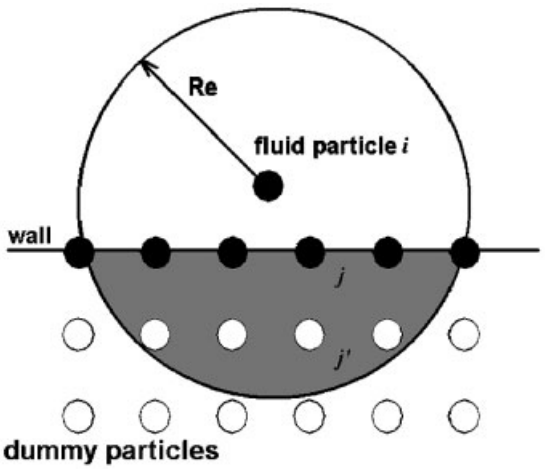

Figure 2. Numerical treatment of pressure boundary conditions.

condition, the temperature of the fictitious particle is the same as that of the corresponding fluid particle.

For the pressure Poisson equation, only fluid and one-layer wall particles are calculated using the ICCG method. Pressure homogeneous Neumann boundary condition is applied between one-layer wall particles and two-layer dummy particles. Figure 2 shows the treatment of the pressure boundary condition for the fluid particle i, where j is the wall particle that lies in the cut-off circle of particle i, and the particle j' lies at a distance of Δl in the normal direction to the wall boundary from wall particle j. According to the pressure Neumann boundary condition, the pressures of particles j and j' should be the same. Particle i will interact with particle j' in both the pressure gradient model and the pressure Poisson equation.

3. NUMERICAL TESTS FOR IMPROVED MPS METHOD

Three numerical tests were performed to demonstrate the effectiveness of our improved MPS method described above. In this section, the results of numerical tests were presented in comparison with exact analytical solutions.

3.1. Heat conduction in a square slab

Heat conduction in a homogeneous square slab was simulated with an initial sinusoidal temperature distribution. The top and bottom edges and lateral sides were assumed to be adiabatic and isothermal, respectively. For this problem, the exact solution is given by Cleary [11]

$$T(x, y, t) = \sin\left(\frac{\pi x}{l}\right)\exp\left[-\left(\frac{\pi}{l}\right)^2 \alpha t\right] \tag{24}$$

where l is the length of the slab and α is the thermal diffusivity. In the present simulation, the slab was modelled by a particle array of 40×40 with $l = 0.1$ m and $\alpha = 0.1\ \mathrm{m^2\ s^{-1}}$. The results are shown in Figures 3(a) and (b) in comparison with ones obtained using the original Laplacian model. As is seen from the figures, the original Laplacian model overestimates the heat transfer; however, using the new Laplacian model, the simulation results agree well with the analytical solutions, and the errors in temperature are less than 1% in the simulation.

3.2. One-dimensional heat penetration

A one-dimensional heat penetration into a semi-infinite medium [12] was also calculated. The medium was represented by a particle array of 1000×20 with a thermal diffusivity of $18.7 \times 10^{-6}\ \mathrm{m^2\ s^{-1}}$. The initial temperatures of the wall and medium were 0 and 20°C, respectively. Figure 4 shows the simulation result compared with the exact solutions at 5 s.

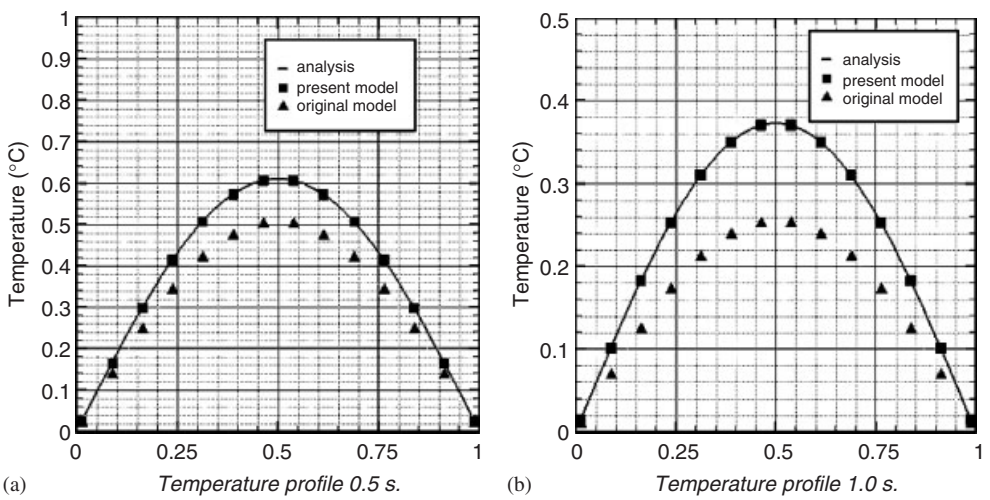

Figure 3. Comparison of temperature for heat conduction in a homogeneous square slab.

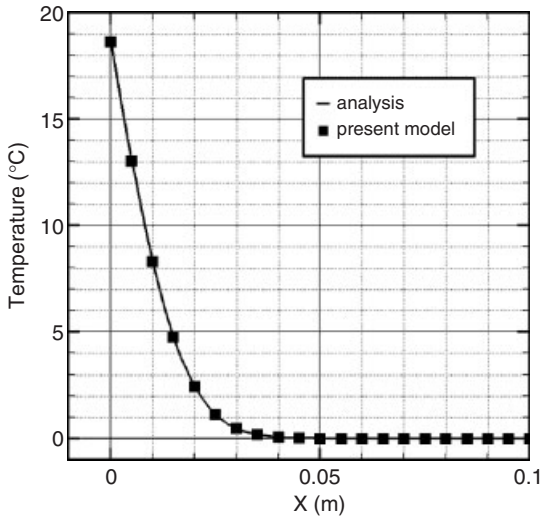

Figure 4. Comparison of temperature profile at 5 s in one-dimensional heat penetration.

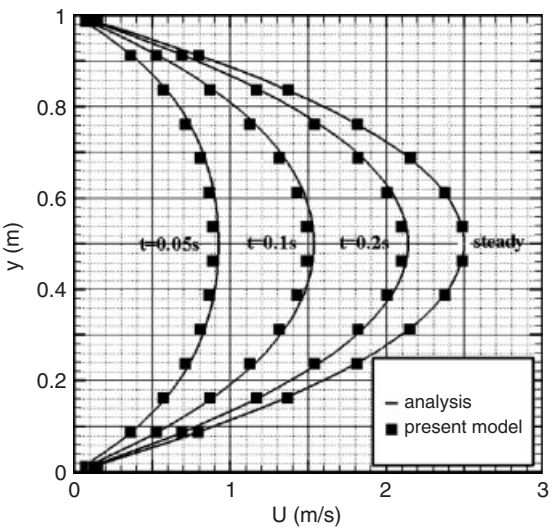

Figure 5. Time-dependent velocity profile in Poiseuille flow in a parallel plate channel.

As can be seen, there is good agreement between them. This is an accuracy typically seen throughout the simulation.

3.3. Poiseuille flow in a parallel plate channel

A simulation was performed for a Poiseuille flow in a parallel plate channel at a low Reynolds number. A periodic boundary condition was assumed at the channel inlet and exit, while the wall boundaries were set to be non-slip. The series solution for the time-dependent behaviour

of this Poiseuille flow is expressed by Morris *et al.* [13]

$$u_y(x,t) = \frac{F}{2\upsilon} y(y-l) + \sum_{n=0}^{\infty} \frac{4Fl^2}{\upsilon\pi^3(2n+1)^3} \sin\left(\frac{\pi x}{l}(2n+1)\right)\exp\left(-\frac{(2n+1)^2\upsilon\pi^2}{l^2}t\right) \quad (25)$$

where x is the coordinate in the flow direction, y is the coordinate normal to the plate, F is the driven body force, l is the channel width and υ is the kinematic viscosity. In the present simulation, $l = 1.0 \times 10^{-3}$ m, $\upsilon = 1.0 \times 10^{-3}$ m^2 s^{-1}, and $F = 0.2 \times 10^5$ m s^{-2} were chosen. A flow channel with a length of 0.5×10^{-3} m length and fluid density of 1.0×10^3 kg m^{-3} was modelled by a particle array of 20×40. The results of calculations of the velocity profile at $x = 0.25 \times 10^{-3}$ m are shown in Figure 5. Comparison with the analytical results indicates excellent agreement.

4. NUMERICAL SIMULATIONS OF RAYLEIGH–BENARD CONVECTION

4.1. Analytical model

Rayleigh–Benard convection in a horizontal layer was simulated with the Boussinesq approximation using present MPS method. The external volume force in Equation (2) is expressed by the buoyancy force [14]

$$\mathbf{F} = \beta\mathbf{g}(T - T_r) \quad (26)$$

where $\mathbf{F}$ is the acceleration due to gravity, T_r is the reference temperature that is equal to the average value of the top and bottom temperature, and β is the thermal expansion coefficient.

Periodic boundary conditions were applied for the lateral walls. The thermal and non-slip boundary conditions of upper and bottom walls were kept with fictitious particles obtained by the reflection of the fluid particles according to the walls. The value of the fictitious particle's velocity was equal to the reflected fluid particles while the direction was opposite. The temperature of the fictitious particle was chosen to keep the wall temperature constant. Fluid particles interacted with other fluid, wall and fictitious particles.

The linear stability theory has shown that the critical wave number k_c for Rayleigh–Benard convection between two rigid boundaries is 3.117 [15], which results in the following critical Rayleigh number:

$$Ra_c = \frac{g\beta\Delta T H^3}{\upsilon\alpha} = 1708 \quad (27)$$

where H and ΔT are the height and the temperature difference between the upper and bottom walls, respectively. The horizontal dimension of the roll is determined by the wavelength $\lambda_c = 2\pi/k_c = 2.016$, which implies the aspect ratio with which the convection roll most readily develops. In the present simulations, therefore, the horizontal layer filled with air, of which Prandtl number is 0.71, was modelled by a two-dimensional geometry with an aspect ratio H/L of 0.5. The fluid particles in the horizontal layer were represented by a particle array of 80×41 including the inner wall particles.

A stable conduction exists for this problem when the temperature difference between the bottom and top boundaries is small enough. However, when the temperature difference is increased above a certain threshold, the static conduction becomes unstable against any small disturbance, and the system then becomes unstable. Calculations started from a static state except for the pressure field, which was perturbed as

$$p(x, y) = \left[1 + \frac{\rho\beta g\Delta T y}{2}\left(1 - \frac{y}{H}\right)\right]\left[1 + 0.001\ \cos\left(\frac{2\pi x}{L}\right)\right] \tag{28}$$

4.2. Calculation of results and analysis

Cell patterns, the critical Rayleigh number and heat flux appear the most interesting aspects of research regarding Rayleigh–Benard convection. Present simulations showed the roll pattern; according to linear theory, the width of rolls should be equal to the wavelength of the disturbance [6]. This means that there should be two cells developed in two-dimensional simulations, and the present simulations showed two cells developed after the fluids were steady.

The enhancement of the heat transfer can be described by the Nusselt number:

$$Nu = 1 + \frac{\langle u_y T\rangle}{\alpha\Delta T/H} \tag{29}$$

where u_y is vertical velocity, α is thermal diffusivity and $\langle\cdot\rangle$ the average over the whole flow domain. Figure 6 shows heat transfer transient from conduction to convection as the Rayleigh number increases. When the Rayleigh number is less than 2000, the averaged Nusselt number is almost equal to 1.0, which means that heat conduction is dominant at this stage. When the Rayleigh number is larger than 2000, the averaged Nusselt number increases rapidly. Mainly, heat transfer changes from conduction to convection. Figure 7 shows the velocity

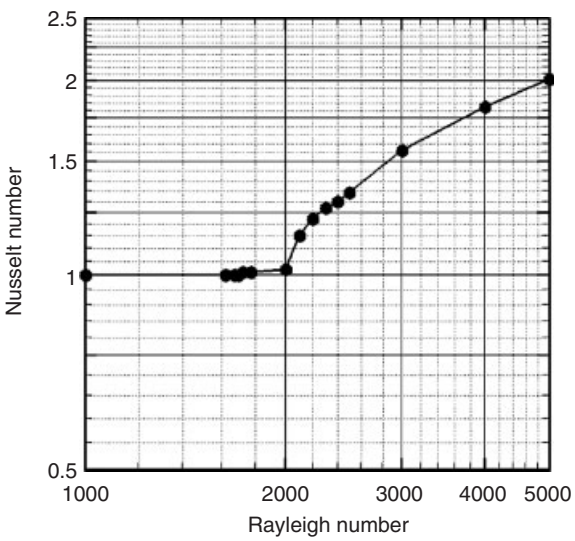

Figure 6. Heat transfer near critical Rayleigh number.

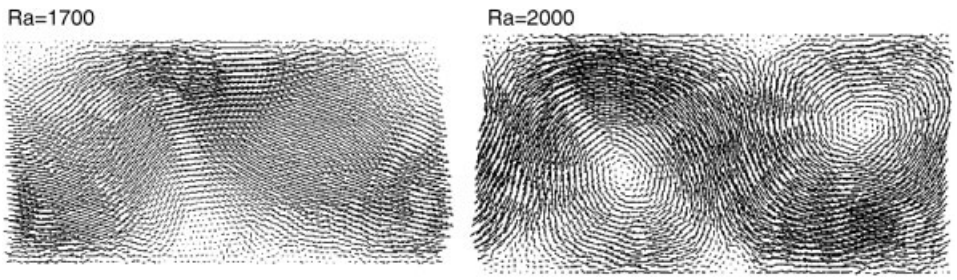

Figure 7. Velocity distribution of Rayleigh–Benard convection ($Ra = 1700$ and 2000).

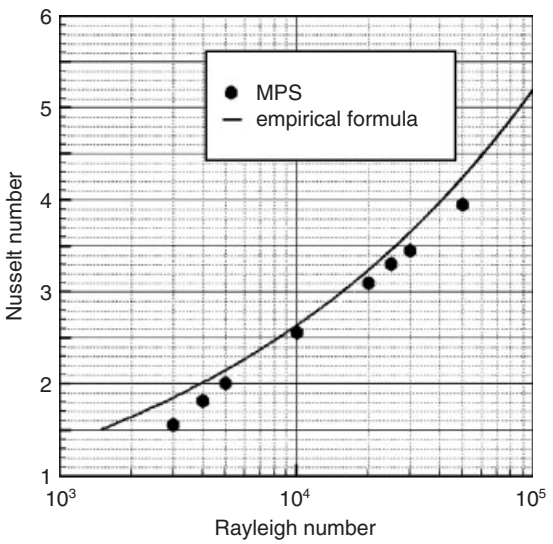

Figure 8. Dependence of Nusselt number on Rayleigh number.

distributions with Rayleigh numbers of 1700 and 2000. It can be seen that convection starts when the Rayleigh number is larger than 2000. Our results suggest that the critical Rayleigh number ranges between 1700 and 2000, which is consistent with the critical Rayleigh number based on Equation (27) of the linear stability theory.

The empirical formula of the dependence of the Nusselt number on the Rayleigh number in the rigid boundary case is [12]

$$Nu = 1.56(Ra/Ra_c)^{0.296} \tag{30}$$

where

$$Ra = \frac{\beta \Delta T g H^3}{\upsilon \alpha} \tag{31}$$

This empirical formula well represents heat transfer in Rayleigh–Benard convection with moderate Rayleigh numbers. In Figure 8, the Nusselt number as a function of the Rayleigh number is compared between the present simulations and empirical formulae. Agreement is found at

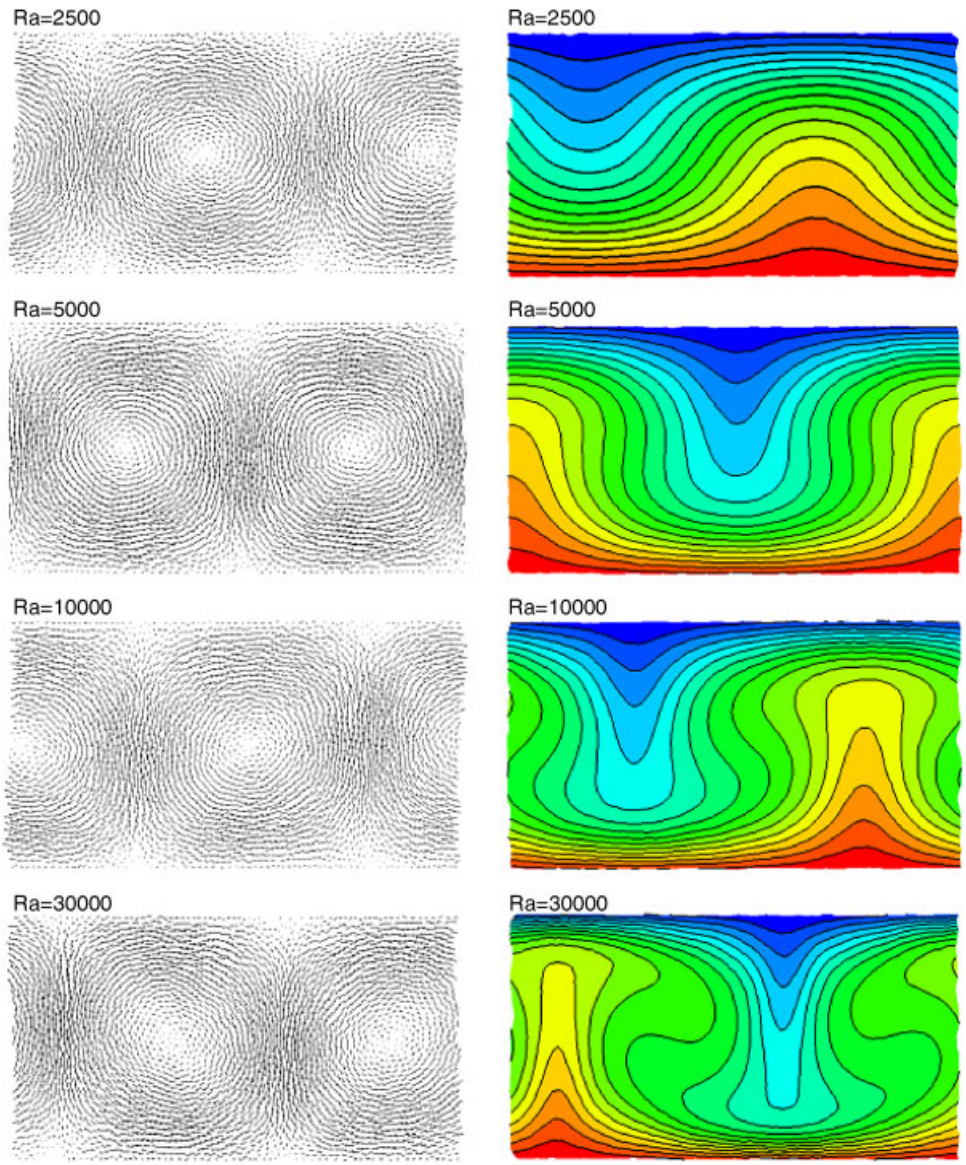

Figure 9. Velocity distribution and temperature contour of Rayleigh–Benard convection ($Ra = 2500, 5000, 10\,000$ and $30\,000$).

Rayleigh numbers between 5000 and 20 000, which is consistent with the results obtained by the lattice Boltzmann method [16]. The comparison indicates that the present MPS can reasonably predict the development of heat transfer in Rayleigh–Benard convection. Figure 9 shows steady velocity distribution and temperature contours, from which it can be concluded that the temperature gradient near the bottom and top boundaries increases as the Rayleigh number increases.

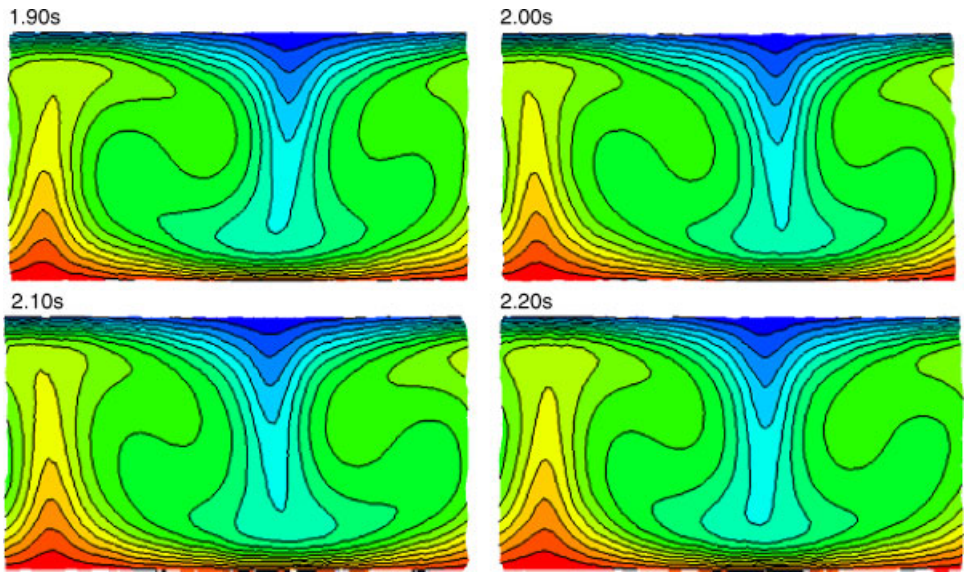

Figure 10. Oscillatory state of Rayleigh–Benard convection ($Ra = 50\,000$).

The two-dimensional convection pattern characterized by the rolls is unstable at higher Rayleigh numbers. Previous work has shown that Rayleigh–Benard convection would evolve into an oscillatory state if the simulation starts from a static conductive state with $Ra > 30\,000$ [16]. These phenomena are observed in present simulation when the Rayleigh number is 50 000, as shown in Figure 10.

The MPS method is a fully Lagrangian method, and so can be used to observe details of the transient flow of cells. Figure 11 shows the start and development of Rayleigh–Benard convection at $Ra = 50\,000$. At the beginning, a dextral cell is developed in the lateral sides. Clockwise and dextral cells develop in the inner left-upper and right-bottom corners, respectively. This can be observed in the simulation result at 0.75 s. From 0.75 to 0.85 s, these two inner cells join in the enhancement of the heat transfer. This coalescent inner cell continues growing larger and rotating before 1.0 s. After 1.0 s, the size of the inner and side cells does not change significantly; however, both these cells rotate all the time until a steady state is achieved, which can be seen from the results at 1.25 and 1.75 s.

Three-dimensional simulations were also performed to demonstrate the effectiveness of the improved MPS on the simulation of Rayleigh–Benard convection. The horizontal layer was modelled by a three-dimensional geometry with an aspect ratio of 2:2:1 ($H:W:L$). In the calculation, Rayleigh number and Prandtl number were fixed as 6000 and 0.71, respectively. Two particle arrays, $40 \times 40 \times 21$ and $60 \times 60 \times 31$ including inner wall particles, were tested to investigate the effect of special resolution on simulation results. Figures 12 and 13 show the steady temperature contour at the middle height of the horizontal layer and the steady velocity distribution, respectively. The results were obtained using the particle array of $60 \times 60 \times 31$. As shown in these figures, horizontal roll cells developed in the fluid layer after the achievement of a steady state under the present conditions. Nusselt numbers obtained with these two

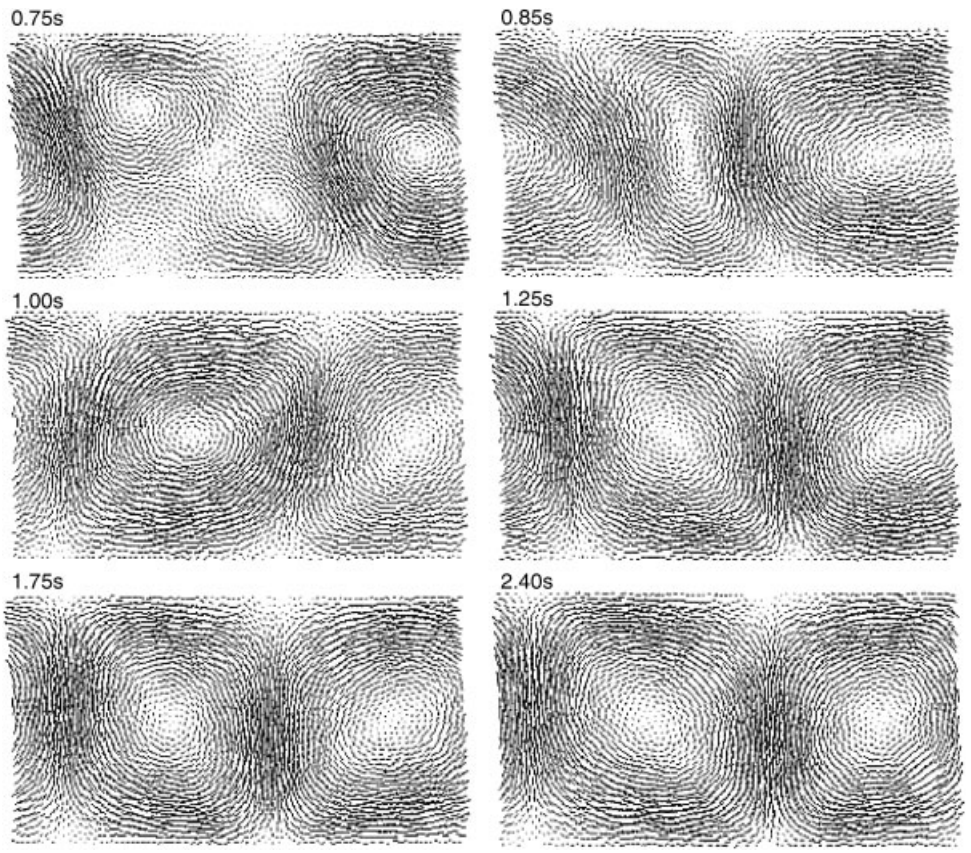

Figure 11. Velocity distribution of Rayleigh–Benard convection at selected time intervals ($Ra = 50\,000$).

particle-array arrangements were 2.093 and 2.151, respectively. The empirical formula yields $Nu = 2.262$. These mean that the error between simulations and the empirical formula would decrease as the number of particles used in the simulation increases. On the other hand, there is less difference in the roll patterns appearing in the horizontal layer between two results obtained by different particle-array arrangements. The simulation results on the roll pattern were in good agreement with those obtained by other numerical methods [17].

5. CONCLUSION

In this paper, we presented an improved MPS method using a new Laplacian model and a new method of treating boundary conditions for numerical simulations of convective heat transfer problems. Several numerical tests indicated the validity of the present model and method for the heat transfer and viscous flow problems by comparisons with exact solutions. Rayleigh–Benard convection with different Rayleigh numbers was also successfully simulated. The simulation results were consistent with those obtained by previous studies and linear the-

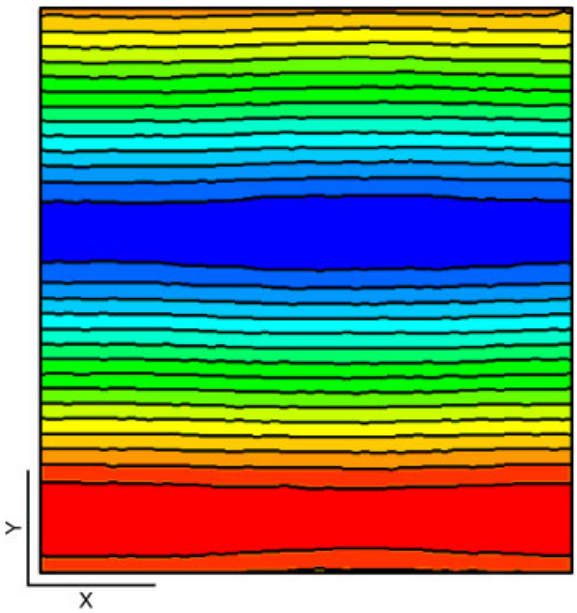

Figure 12. Steady temperature contour of Rayleigh–Benard convection at the middle height of horizontal plane (Three-dimensional simulation with $Ra = 6000$).

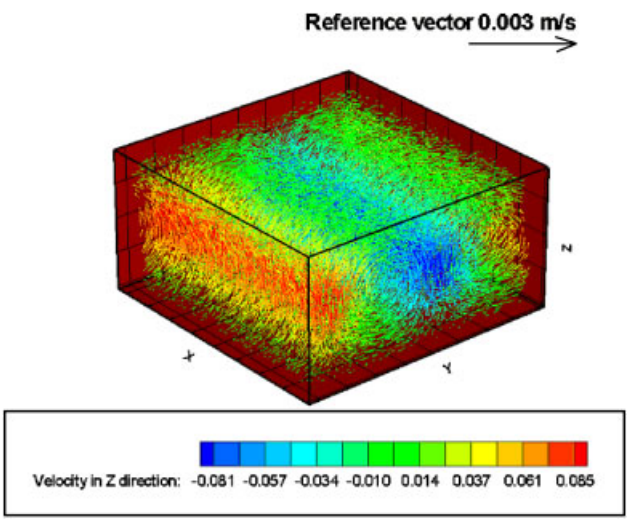

Figure 13. Steady velocity distribution of Rayleigh–Benard convection (Three-dimensional simulation with $Ra = 6000$).

ory. Dependence of the Nusselt number on the Rayleigh number agreed well with an empirical formula. The steady temperature contour and velocity distribution agreed well with other simulation results. The start and development of Rayleigh–Benard convection can be reproduced reasonably with the present MPS method. The roll pattern developed in the horizontal fluid layer as well as the convective heat transfer was successfully simulated with three-dimensional MPS calculations. It is thus expected that our improved MPS method presented here will be a powerful tool to analyse convective heat transfer problems.

NOMENCLATURE

c_p	specific heat at constant pressure ($J\,kg^{-1}K^{-1}$)
d	spatial dimensions
F	external volume force or driven force ($m\,s^{-2}$)
H	height (m)
k	thermal conductivity ($W\,m^{-1}k^{-1}$)
l, L	length (m)
n^0	initial number density
n^*	temporary number density
Nu	Nusselt number
p	pressure (Pa)
q	energy transfer rate per unit volume ($W\,m^{-3}$)
r	position vector (m)
Ra	Rayleigh Number
r_e	cut-off radius of the kernel function
T	temperature (K)
t	time (s)
u	velocity ($m\,s^{-1}$)
v	volume (m^3)
w	kernel function
W	width (m)

Greek letters

α_1, α_2	tuning parameters in the Poisson equation
β	thermal expansion
λ	tuning parameter in the Laplacian model
φ	arbitrary vector variable
Φ	arbitrary scalar quantity
ρ	density ($kg\,m^{-3}$)
υ	kinematic viscosity ($m^2\,s^{-1}$)
Δl	initial distance between two particles
Δt	time step size (s)

Subscripts

i, j	particle number

ACKNOWLEDGEMENTS

One of the authors, Shuai Zhang, gratefully acknowledges support from the Ministry of Education, Culture, Sports, Science and Technology, Japan under the MONBUKAGAKUSHO Scholarship.

REFERENCES

1. Koshizuka S, Oka Y. Moving-particle semi-implicit method for fragmentation of incompressible fluid. *Nuclear Science and Engineering* 1996; **123**:421–434.
2. Yoon HY, Koshizuka S, Oka Y. A particle-gridless hybrid method for incompressible flows. *International Journal for Numerical Methods in Fluids* 1999; **30**:407–424.
3. Shirakawa N, Yamamoto Y, Horie H, Tsunoyama S. Analysis of flows around a BWR spacer by the two-fluid particle interaction method. *Journal of Nuclear Science and Technology* 2002; **39**(4):572–581.
4. Chandrasekhar S. *Hydrodynamic and Hydromagnetic Stability*. Dover: New York, 1990.
5. Cross MC, Hohenberg PC. Pattern formation outside of equilibrium. *Reviews of Modern Physics* 1993; **65**:851–863.
6. Mareschal M, Kestermont E. Experimental evidence for convective rolls in finite two-dimensional molecular models. *Nature* 1987; **329**:427–429.
7. Watanabe T, Kaburaki H, Machida M, Yokokawa M. Growth of long-range in a transition between heat conduction and convection. *Physical Review E* 1995; **52**:1601–1605.
8. He X, Chen S, Doolen GD. A novel thermal model for the lattice Boltzmann method in incompressible limit. *Journal of Computational Physics* 1998; **146**:282–300.
9. Kum O, Hoover WG. Viscous conducting flows with smooth-particle applied mechanics. *Physical Review E* 1995; **52**:4899–4908.
10. Ikeda H. Numerical analysis of fragmentation processes in vapor explosion using particle method. *Doctoral Thesis 1999*, Tokyo University, Japan (in Japanese).
11. Cleary PW. Modelling confined multi-material heat and mass flows using SPH. *Applied Mathematical Modelling* 1998; **22**:981–993.
12. Beek WJ, Muttzall KMK, Van Heuven JW. *Transport Phenomena* (2nd edn). Wiley: Chichester, 2000.
13. Morris JP, Fox PJ, Zhu Y. Modeling low Reynolds number incompressible flows using SPH. *Journal of Computational Physics* 1997; **136**:214–226.
14. Koshizuka S, Yoon HY, Yamashita D, Oka Y. Numerical analysis of natural convection in a square cavity using MPS-MAFL. *Journal of Computational Fluid Dynamics* 2000; **8**(4):485–494.
15. Reid WH, Harris DL. Some further results on the Benard problem. *Physics of Fluids* 1958; **1**(2):102–110.
16. Shan X. Simulation of Rayleigh–Benard convection using a lattice Boltzmann method. *Physical Review E* 1997; **55**(3):2780–2788.
17. Watanabe T. Flow pattern and heat transfer rate in Rayleigh–Benard convection. *Physics of Fluids* 2004; **16**(4):972–978.

